Hindawi
Journal of Sensors
Volume 2023, Article ID 3069921, 11 pages
https://doi.org/10.1155/2023/3069921

Research Article

Satellite-Synoptic Monitoring of Dominant Dust Entering Western Iran

Himan Shahabi,[1] **Taher Safarrad**,[2] **Mazlan Hashim**,[3,4] **and Nadhir Al-Ansari**[5]

[1]*Department of Geomorphology, Faculty of Natural Resources, University of Kurdistan, Sanandaj 66177–15175, Iran*
[2]*Geography and Urban Planning Department, University of Mazandaran, Babolsar 13534–47416, Iran*
[3]*Geoscience and Digital Earth Centre (INSTeG), Research Institute for Sustainability and Environment (RISE), Universiti Teknologi Malaysia, 81310, UTM Johor Bahru, Malaysia*
[4]*Faculty of Built Environment and Surveying, Universiti Teknologi Malaysia (UTM), Johor Bahru 81310, Malaysia*
[5]*Department of Civil, Environmental and Natural Resources Engineering, Lulea University of Technology, 97187, Lulea, Sweden*

Correspondence should be addressed to Himan Shahabi; h.shahabi@uok.ac.ir

Received 2 June 2023; Revised 28 July 2023; Accepted 28 August 2023; Published 19 September 2023

Academic Editor: Rajkishor Kumar

Dust storm in Iran's western regions has been one of its major environmental problems in recent years, which has not only turned into a yearly phenomenon but is also expanding. This study investigated two events of dominant dust in southwestern Iran using moderate resolution imaging spectroradiometer imagery, Reanalysis Datasets (meteorological fields and atmospheric compositions), in both hot (July 2, 2008) and cold (February 18, 2017) seasons. After radiometric correction and calculation of brightness temperature as well as the reflective and thermal behavior of dust, the research results showed that the detection of dominant dust entering was 0.645 μm (visible red) and 0.858 μm (near-infrared) in the reflective ranges and 3.959, 8.55, 11.03, and 12.02 μm in the thermal ranges. Synoptically, the lower values for mean sea level pressure from the east Mediterranean along Syria and Iraq to the southwest and Central Asia facilitate a convergence condition in the lower troposphere that induces strong northwesterlies, Shamal winds, over the Middle East toward the Persian Gulf, forming a more expansive aerosol hotspot over southwest Iran. However, on a cold day, high dust events in Arabia and south Iran are related to the ongoing high pressure, which is accompanied by a subtropical jet, following anticyclonic circulation toward southwestern Iran.

1. Introduction

As a climatic phenomenon, dust is driven by natural and anthropogenic factors and can disturb human activities and social and industrial infrastructures [1–2]. The large volume of particles transported to the troposphere can alter the energy balance and ultimately the climatic conditions of the regions [3–4]. Human intervention in the natural environment is one of the main drivers of increased dust sources and emissions [5, 6]. Prospero et al. [7] identified the main Middle Eastern dust sources as the Empty Quarter in Saudi Arabia, the dry lowlands of the banks of the Tigris and Euphrates rivers, and the coasts of the Oman Sea. These sources are part of a dust belt stretching from the northwest coastal area of Africa to the Middle East along Central Asia to China [8–10]. The optical properties of dust particles (observed satellite radiance) make it possible to distinguish them from other phenomena [11]. Many detection methods use reflectance in visible bands and brightness temperature (BT) in infrared bands. The difference in BT in different bands is a suitable method for distinguishing dust from other phenomena.

Since 1970, researchers have been able to determine the occurrence of dust storms through visible and near-infrared and thermal infrared. Shenk and Curran [12] applied image enhancement to dust storms over land and water using visible and infrared satellite measurements. Ackerman [13] proposed the application of BT to detect different phenomena. In addition, Miller [14] used two different algorithms for the image enhancement of dust. He used the reflective properties of 0.46 and 0.85 μm spectral ranges for image enhancement of dust over water and the BT in 11 and 12 μm spectral ranges over desert areas. Chen et al. [15] used moderate

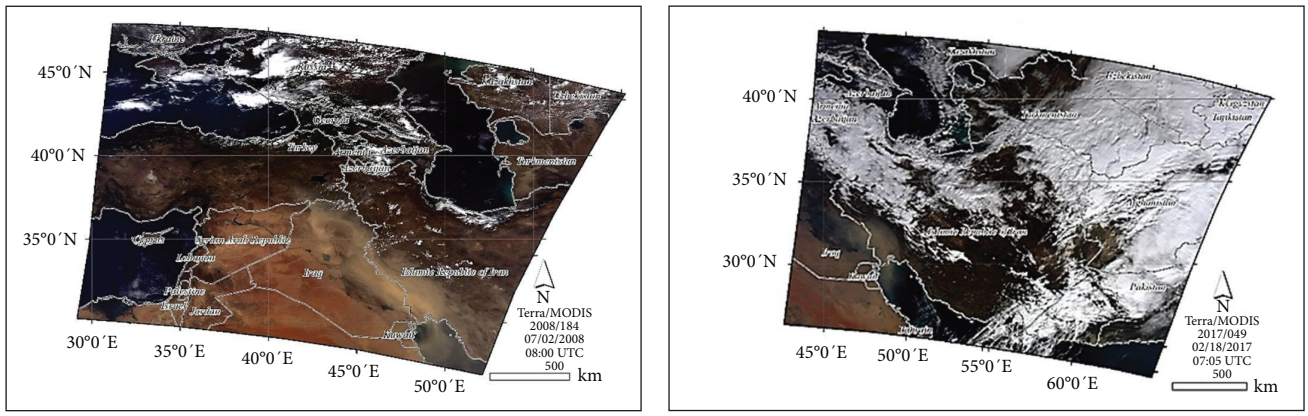

(a) (b)

Figure 1: True color images (143): (a) July 2, 2008, and (b) February 18, 2017.

resolution imaging spectroradiometer (MODIS) visible and infrared images and AMSR-E microwave images for the enhancement of dust masses in northwest China. They detected dust masses under ice clouds using microwave images and visible and infrared data during clear sky conditions and defined a microwave polarization index. Their image enhancement was based on the calculation of the polarized brightness temperature difference (BTD) between 89 and 8.23 GHz frequencies and the BTD between 11 and 12 μm wavelengths [16]. These included false color composite (FCC), BTD, Ackerman's method, Miller's recurrence algorithm, and the Roskavensky method. In addition to these methods, the ozone monitoring instrument (OMI) aerosol index was calculated for all dust as an independent assessment source. They applied these algorithms to a study of four major dust storms in Australia. Their results showed that all methods performed better than FCC, but it was not possible to present a single method for all storm types. This is due to factors such as the presence of cloud cover, variations in the mineral structure of particles, and reflective surface changes. Klüser and Schepanski [17], using Meteosat Second Generation infrared images, developed a bitemporal mineral dust index and prepared a time series of 2006 for four desert regions. The comparison of the results from this index with MODIS and OMI satellite data and AERONET ground data showed the high capability of this index in detecting dust masses and estimating the continental and desert surface sediment load, except for regions with high relative humidity.

According to a review of earlier scientific publications, there is some unclassified information regarding the synoptic pattern of these dust storms [18, 19]. Furthermore, there is no quantitative distinction between the locations of high and low-pressure systems in severe dust storms [20–21]. Therefore, having sufficient knowledge of the synoptic state of different types of dust storms is the first step to a succinct and appropriate analysis of dust storms [22].

On the other hand, many indices have been used for dust detection, including infrared differential dust index [23], normalized differential dust index (NDDI; [24]), mean normalized difference vegetation index [25], aerosol absorption index, and aerosol optical depth (AOD) [26]. Dust storms, as a most common climatic phenomena in arid and semi-arid desert areas, are widespread across the Middle East to East of Asia [7, 27]; among them, the Middle East (including sources of Iraq–Syria, Arabian Peninsula, Iran desserts) is not only one of the major sources of mineral dust, but also it is one of the regions that are affected by severe dust storms [28–32]. The behavior of mineral dust in the region (emission, transport, and accumulation) is mostly caused by mesoscale atmospheric circulation, which also accounts for a substantial portion of dust storms [33–36]. In addition, Data from ground measurements, remote sensing, and reanalysis over the regions demonstrated that the seasonally dynamic–synoptic circumstances cause different dust storms [37–40].

Dust detection using satellite images is dependent on place and time. Therefore, it is not possible to present a single algorithm for global detection, and different methods and thresholds should be used for different times and places. The present study aims to investigate the dust masses entering Iran from the southwest using the reflective and thermal properties of MODIS imagery in cold and hot seasons. Furthermore, in this study, the utilization of reflecting and thermal properties is examined simultaneously for detecting dust through MODIS satellite imagery. The results will be used to improve the synoptic analysis of dust occurrence, and the dust origin will be described using the HYSPLIT model. It is noted that the phenomena of dust and its various properties will be examined in this study using a combined perspective (satellite detection, synoptic analysis, and the HYSPLIT model).

2. Datasets

2.1. MODIS Images. This study used MODIS imagery for dust detection. The images were selected such that dust exists in land and sea together with other phenomena having spectral interference with dust (e.g., clouds, snow, barren land, desert, vegetation, and water bodies). Here, two images from July 2, 2008, and February 18, 2017, were selected in warm and cold seasons, respectively, in southwestern Iran (Figure 1).

The European Centre for Medium-Range Weather Forecasts updated the ECMWF reanalysis (ERA) Interim reanalysis with the ERA-5 reanalysis, which has a detailed record of

the global atmosphere, land surface, and ocean waves from 1950 onward [41]. The most current datasets provide an ensemble at 3 hr and two sets of hourly reanalyses, with characteristics including 31 km horizontal resolution and 137 levels ranging from the surface to 0.01 hPa [41]. This study used meteorological fields from the ERA-5 reanalysis (mean sea level pressure (MSLP), zonal wind at 250 hPa, geopotential heights at 850 and 500 hPa, and vector winds at 10 m) to assess the characterization of the synoptic conditions at $0.75^\circ \times 0.75^\circ$ spatial resolution over the study region (10°E–65°E, 10°N–55°N).

The most recent worldwide data set of atmospheric composition (AC) provided by CAMS (Copernicus Atmosphere Monitoring Service) is known as CAMS reanalysis [42]. It consists of 3D time-consistent AC fields. A 4D variational analysis with a 12-hr analysis window is part of the CAMS data, which is based on the modeling of aerosols from various sources and satellite data (MODIS AOD550nm) assimilation [43, 44]. This analysis provides dust-AOD at 550 nm, which has recently been validated against MERRA-2 and ground-based measurements [45]. Therefore, dust AOD (DAOD550nm) is the term employed in this study to describe how well dust particles at a spatial resolution of $0.5^\circ \times 0.5^\circ$ obstruct solar radiation energy from reaching the surface.

3. Detection Methodology

The true color images of the MODIS sensor obtained by the NASA website (https://search.earthdata.nasa.gov) provide 143 images, covering the study area. Therefore, two episodes, out of the study cases, including (a) July 2, 2008, and (b) February 18, 2017, are analyzed [46].

It is noted that by examining the spectral behavior of dust and other phenomena in the applied satellite imagery, it was found that dust in the visible and red ($\rho_{0.645\,\mu m}$) and near-infrared ($\rho_{0.858\,\mu m}$) ranges can be separated from other phenomena by applying thresholds. The threshold value depends on the season, and in the cold season, due to the reduction of vegetation on the ground, it takes smaller values. In this research, the following thresholds were applied to the reflective ranges:

$$\rho_{0.858\,\mu m} < (0.35 \text{ in winter}), (0.55 \text{ in summer}). \quad (1)$$

$$\rho_{0.645\,\mu m} > (0.15 \text{ in winter}), (0.2 \text{ in summer}). \quad (2)$$

The BT is one of the best and most highly effective variables for dust detection. The analysis of the target range will show that the simultaneous use of 3.959, 8.55, 11.03, and 12.02 μm spectral ranges provided the best results given the high complexity of the study area, which included water bodies, barren land, desert, vegetation, and clouds all together alongside dust. This makes it impossible to separate the dust based on only one thermal range. Here, BT was employed in the specified ranges by applying thresholds as per the following equations:

$$\left(BT_{8.55\,\mu m} - BT_{11.03\,\mu m}\right) - \left(BT_{11.03\,\mu m} - BT_{12.02\,\mu m}\right) > -0.5^\circ K. \quad (3)$$

$$\left(BT_{12.02\,\mu m} - BT_{11.03\,\mu m}\right) > 0^\circ K. \quad (4)$$

$$\left(BT_{3.959\,\mu m} - BT_{11.03\,\mu m}\right) > 5^\circ K. \quad (5)$$

An investigation of the spectral behavior of dust and other phenomena in the selected images shows that dust can be separated from other phenomena in the visible red ($\rho_{0.645\,\mu m}$) and near-infrared ($\rho_{0.858\,\mu m}$) ranges. The threshold value depends on the season, with smaller values in the cold season due to the reduction of surface vegetation. Finally, the pixels containing all the mentioned conditions were identified as dust (Figure 2).

4. Results and Discussion

4.1. Spectral and Thermal Behavior of Dust. This study focused on the reflective and thermal properties of dust for dust detection. In the visible range (0.4–0.7 μm), dust showed higher reflection in barren lands, vegetation, and water and lower reflection in clouds and snow. In the mid-and near-infrared range (0.8–2.5 μm), dust reflection increased by increasing wavelength, with the highest reflection in the 2.13 μm range. This makes it difficult to identify the two phenomena (Figure 3). Therefore, visible red (0.645 μm) and near-infrared (0.858 μm) ranges proved more suitable than other spectral ranges, and dust phenomena can be identified suitably by applying appropriate thresholds.

The dust detection over land and water is largely different. As explained above, dust detection was easier over land, whereas its detection over water requires using BT. Many researchers [13, 47, 48] advocate employing BT in the 3.959, 8.55, 11.03, and 12.02 m spectral regions to distinguish dust from other phenomena. Figure 4 illustrates the thermal behavior of dust compared to other phenomena based on the proposed methods.

Finally, threshold values were determined by differentiating between dust and other phenomena in the reflective and thermal ranges. The spectral behavior of the dust and other phenomena in images can be examined, and the set thresholds can be used to distinguish the dust from other phenomena. Still, the threshold value depends on the season, with smaller values in the cold season due to the reduction of surface vegetation.

Investigations into the target range revealed that, given the high complexity of the research region, the simultaneous employment of the 3.959, 8.55, 11.03, and 12.02 m spectral ranges produced the optimum outcome. It is impossible to distinguish between the dust based on a single thermal range when there is also water, barren land, vegetation, clouds, and desert present. Applying criteria to extract pixels recognized as a dust zone allowed the use of BT characteristics in the designated ranges in this case. A comparison of model AOD outputs with Terra-MODIS retrievals shows that despite

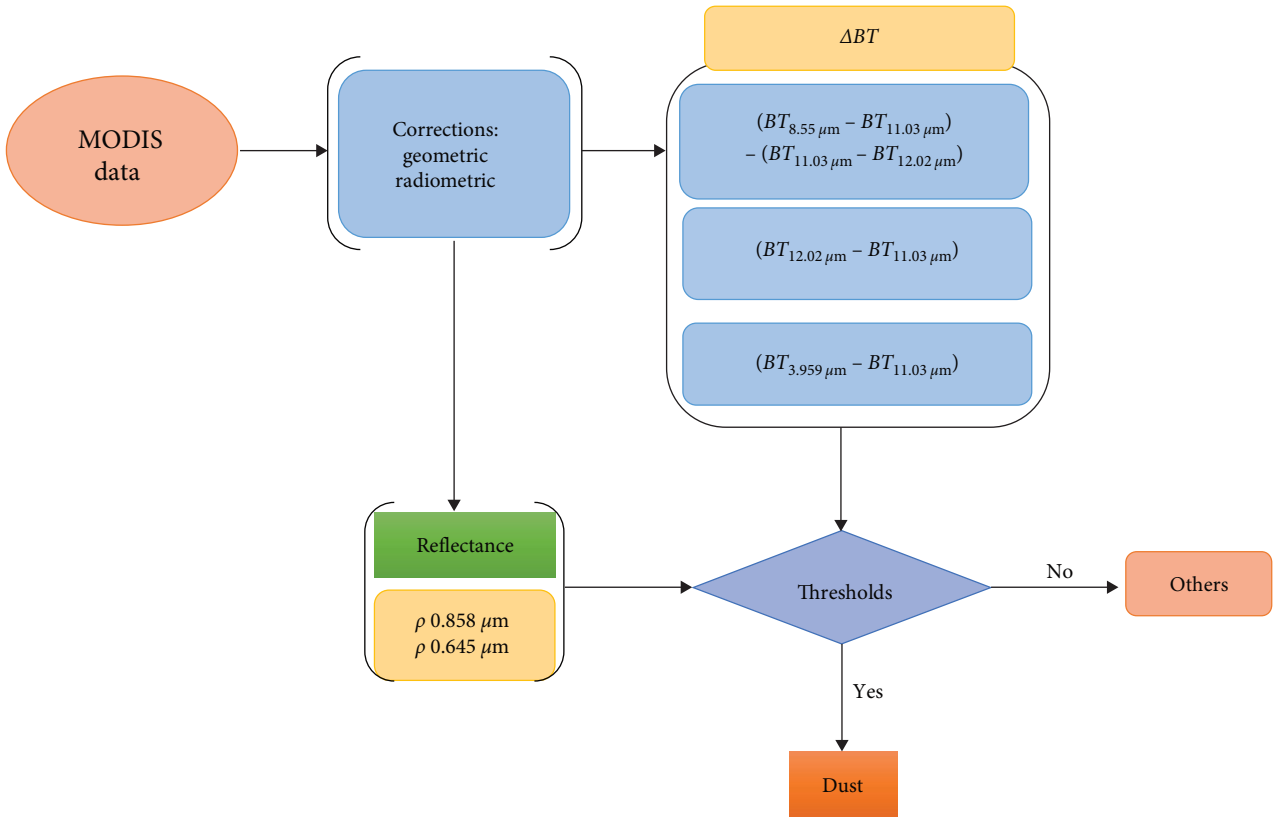

Figure 2: Flowchart of dust detection processing using satellite imagery.

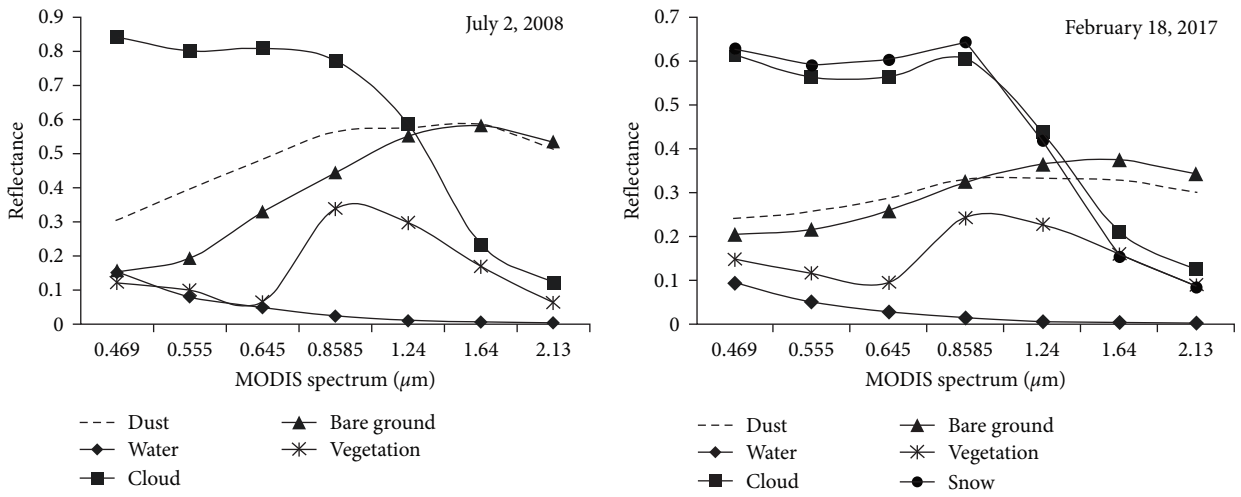

Figure 3: Diagram of the spectral behavior of dust and other phenomena in the two studied images; pure pixels were used to plot the spectral behavior of the phenomena.

significant differences, all models perform fairly well in predicting AOD patterns in the Middle East [40] (Figure 5).

4.2. Synoptic Meteorology Conditions. The synoptic conditions for the cold and warm events that occurred during the episodes with significant dust concentrations in the southwest of Iran are analyzed separately. This aims to explore the atmospheric dynamics, triggering dust storms across the Middle East region that facilitate the transport and accumulation of dust.

4.3. Warm Episode (July 2, 2008). Even though the storm's precise source spots are not evident in this image, the dust looks to have started in northern Iraq. The thickest dust hovers over the border between Iraq and Iran, but a plume of dust also curls over the borders with Syria, Turkey, and

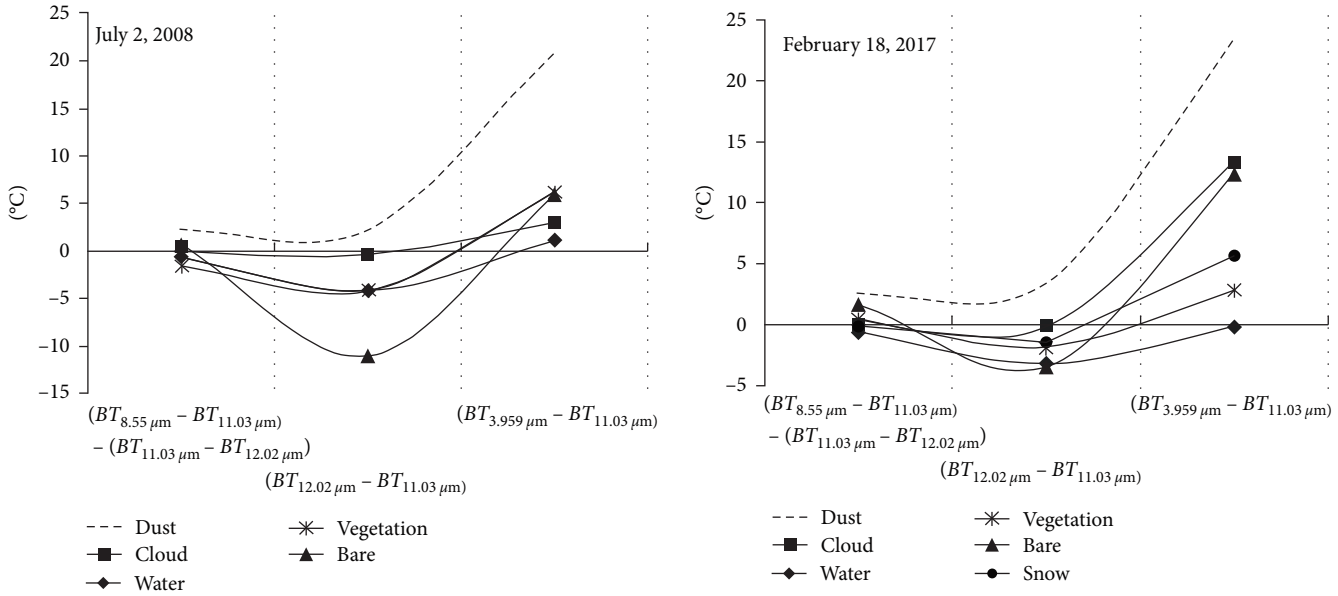

FIGURE 4: The thermal behavior of dust and other phenomena in the two studied images; pure pixels were used to plot the thermal behavior of the phenomena.

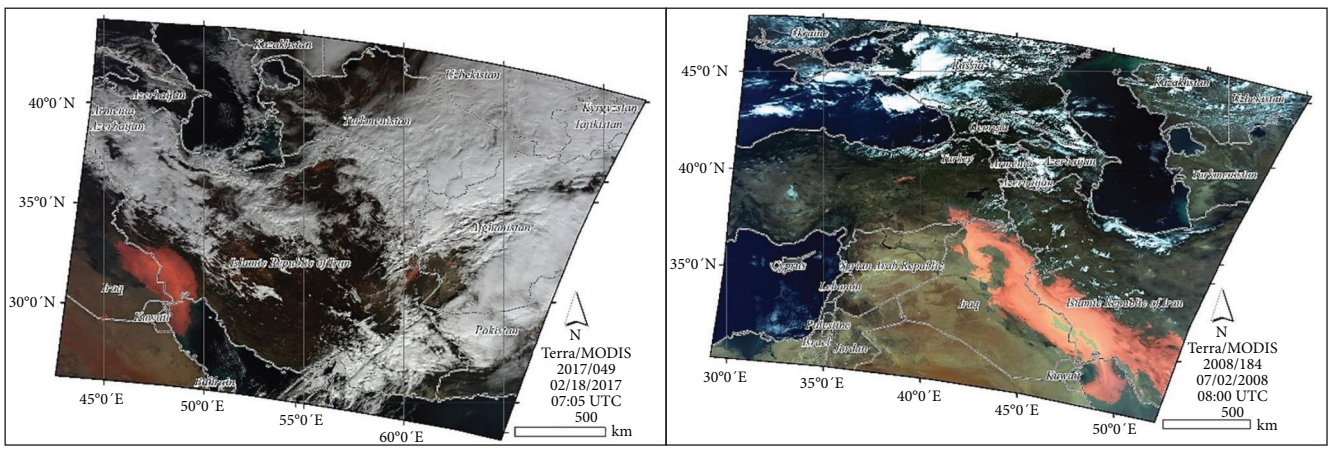

FIGURE 5: Dust detection based on reflective and thermal properties.

Iraq. Dust storm over the Persian Gulf (https://earthobservatory.nasa.gov/images/20175/dust-storm-over-the-Persian-gulf) is caused by fine sediments of the Tigris and Euphrates floodplain [49].

High Caspian Sea-Hindu Kush Index values, which correspond to an enhanced pressure gradient between the Caspian Sea (CS) and Hindu Kush (HK), are linked to the intensification of northerly winds, increased dust emissions, and transportation over SW Asia and the north Arabian Sea, according to satellite remote sensing (Meteosat, OMI, MODIS) analyses [50].

The warming of the earth's surface in arid regions devoid of vegetation is the primary cause of dust in the southwest of Iran during the summer [25]. More recent studies take into account the function of the convergence of south/southwest winds, influenced by the low thermal pressure of the earth's surface in the southern Arabian Peninsula, as the cause of dust transfer to the southwest of Iran [51, 52].

Shamal, a wind from the northwest that frequently blows over the floodplain of the Tigris and Euphrates Rivers in Iraq, is the cause of these thick plumes. The fine sediments in this floodplain provide the area's dust storms in the region.

The lower G850 (1,430 gpm) and MSLP (1005) values covering Turkey, Syria, and Iraq to the southwest and Central Asia (Figure 6(a)) promote ascending conditions in the lower troposphere, while high G850 and MSLP dominate over north Africa and Europe. Strong northerlies from the Aegean Sea to the Middle East are pro-generated as a result of these conditions converging as strong westerlies in the Iran–Iraq boundaries, which eventually changed to enhanced surface westerlies over the area [53]. Prefrontal dust storms are facilitated toward southwest Iran by the convergence of northwest and

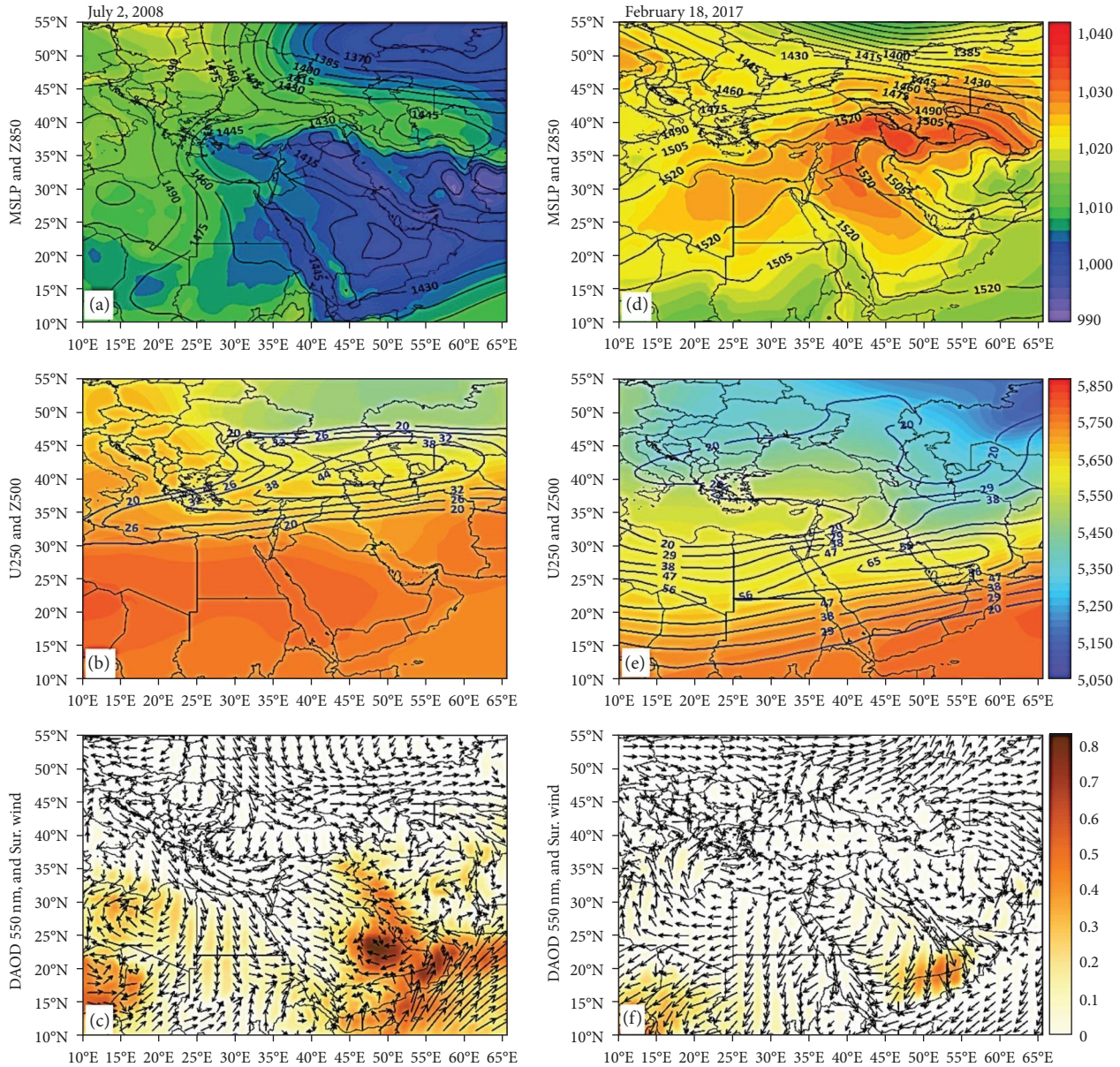

FIGURE 6: Composite synoptic maps of (a and d) MSLP—mean sea-level pressure (shaded area) and geopotential heights at 850 hPa (black contours); (b and e) U-wind at 250 hPa (blue contours) and geopotential heights at 500 hPa (shaded area); (c and f) dust-$AOD_{550\,nm}$ and surface vector winds (in m/s) for the Middle East region during warm (left column) and cold (right column) episodes, respectively.

southwesterly winds as a result of the surface low-pressure in the southern Arabian Peninsula [51, 52] (Figure 6(c)). In general, the meteorological fields created a larger aerosol hotspot over southwest Iran. The surface low-pressure area (Figure 6(a)), also referred to as the Arabian thermal low [54], creates a cyclonic pattern of dust, which causes the southwesterly flow and the northwesterly flow to converge over north Saudi Arabia.

The dust storms across the Sistan basin in eastern Iran were connected to positive anomalies in MSLP and geopotential heights at 700 hPa (Z700) over the CS and negative anomalies over the HK mountain range, according to a recent study [55]. During the long-range transport of a dust storm over the eastern Iranian borders during July 1–3, 2014, a similar synoptic meteorology pattern (i.e., MSLP high over CS and MSLP low over HK) predominated [50, 56] (Figure 6(a)). During this episode day, a subtropical jet stream across the Levantine-Caspian Sea-Turkmenistan and a subtropical ridge (5,750 gpm) over Saudi Arabia and southern Iran are also prominent features (Figure 6(b)). In contrast to the subtropical jet typically linked to high dust events in Arabia and south Iran, which is located around 30°N [57, 58], the zonal 250 hPa winds (subtropical jet) core is located further north during frontal dust storms and cold dust episodes. It reaches a maximum speed of about 44 ms^{-1}. Strong northwesterlies were present over the region and were replaced by southwesterlies in front of

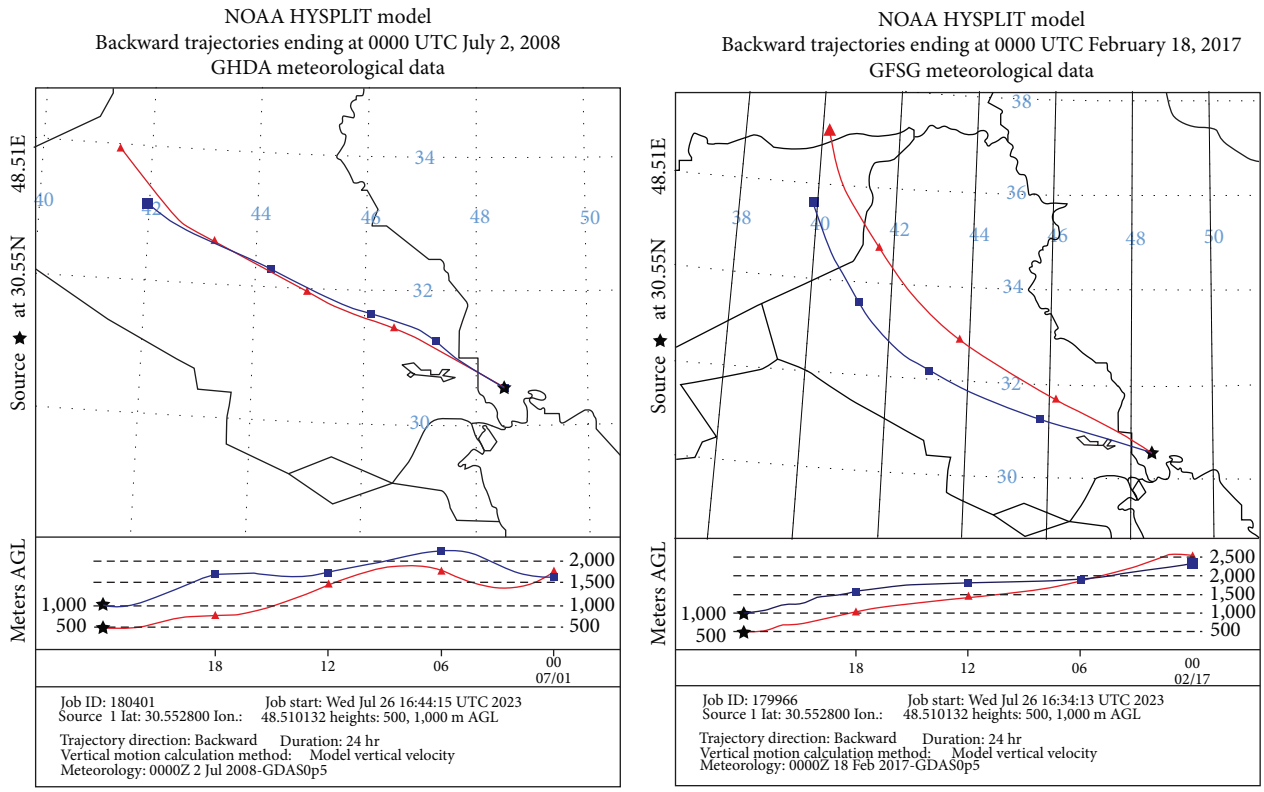

(a) (b)

FIGURE 7: Air flow path, July 2, 2008 (a) and February 18, 2017 (b) based on HYSPLIT model (https://www.arl.noaa.gov/) [65].

the frontal system over central Iran and the southern Arabian Peninsula. High-pressure conditions predominated behind the frontal system over Syria and northwest Iraq [40]. This is a typical MSLP pattern for postfrontal dust storms in the Middle East, which mostly impact the northern Persian Gulf and the Tigris-Euphrates Basin [38].

4.4. Cold Episode (February 18, 2017). The Khuzestan province, northern Kuwait, sections of the Persian Gulf, and parts of Iraq were all affected by the dust storm on February 18, 2017, according to NASA reports (https://earthobservatory.nasa.gov/images/89705/dust-over-the-persian-gulf). According to reports, this dust storm caused electrical infrastructure damage and cutoff power to cities in the Khuzestan region [59]. The air pollution brought on by the dust storm and the power outage in Ahvaz, the capital of Khuzestan, led to a 5-day protest.

Strong shamal winds have a role in dust storms in this area, which often happen during the summer but can also happen occasionally in the winter. According to studies [60, 61], drought and the rise in dust brought on by winter shamal are related.

According to the synoptic study, on February 17, the frontal dust storm's generating low- and high-pressure systems were situated over central Iran and northern Pakistan, respectively. Dust could flourish in this circumstance [62].

Atmospheric circulations on this day are dominated by high MSLP and geopotential values (Figure 6(d)), with a weakened low pressure over Sudan, while a subtropical jet ($>56\,ms^{-1}$) and geopotential values at 500 hPa (Figure 6(e)) associated with dust event in Arabia and southwest Iran in the cold season. A ridge extending from central Asia along to the entire Middle East, along with the development of high pressure over the Caspian Sea and the Middle East and a cold low pressure over the Iran–Afghanistan borders (Figure 6(e)), intensifies air subsidence and facilitates surface northwesterly winds that follow anticyclone circulation and blow toward southwestern Iran while passing through the desert regions of Syria, Iraq, and northern Saudi Arabia. During the cold season, the circumstances created unique dust paths from these regions to SW Iran and Kuwait [63]. In contrast to the warm event on July 2, 2008, the dusty northwest is converging from northeastern Saudi Arabia to southwest Iran with increasing cyclonic activity and a high AOD across the convergence area (Figure 6(f)).

Furthermore, tracking the dust path for southwest Iran using the HYSPLIT model [64] shows that on the days in question, dust entered Iran from the desert areas located in southeast Iraq (Figure 7). The meteorological mechanism that led to the removal of particles and their entry into Iran are different in the two analyzed samples. Based on this, if in the hot season (July 2, 2008) there is a low thermal pressure on the earth's surface, it provides the necessary instability to pick up particles and finally transport them by the westerly to the southwest of Iran (Figure 8(a)). In the cold season (February 18, 2017), the dynamic factor of the upper level of the atmosphere (especially the level of 1,000 and 850 hPa) has provided

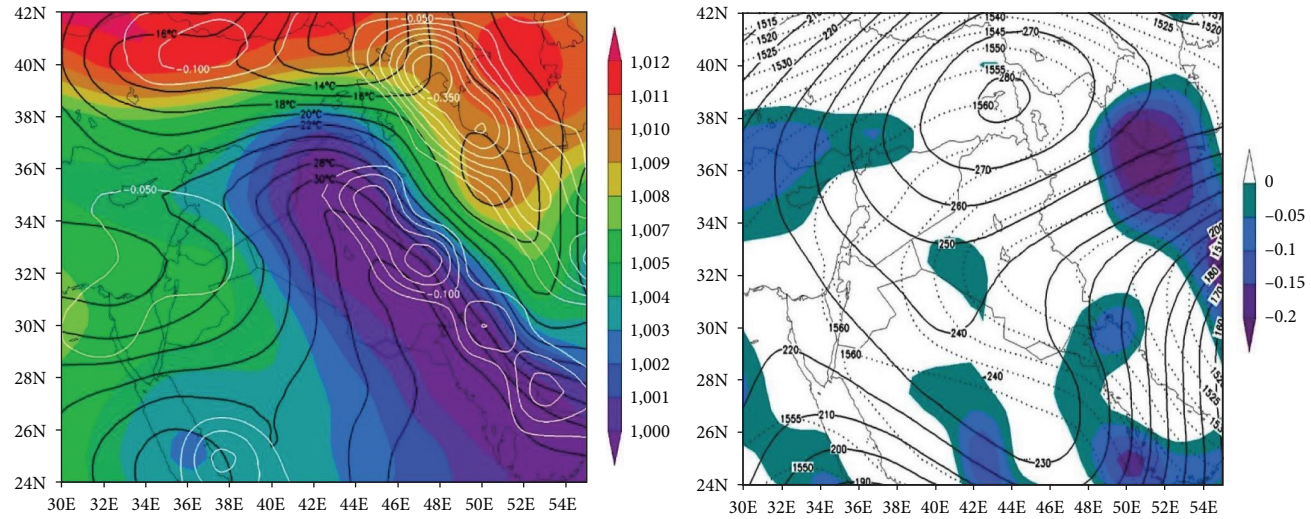

Figure 8: Arrangement of land surface and upper atmosphere patterns for dust event days: (a) July 2, 2008, and (b) February 18, 2017. For map (a): background standardized land surface pressure (SLP) in hPa, black lines, land surface temperature in degrees Celsius and dashed lines, white is Omega in Pascasl/s. For map (b), the background of Omega values in Pascal/s, continuous lines, geopotential height is 1,000 hectopascals in meters and broken lines; geopotential height is 850 hectopascals in meters.

the necessary instability to remove particles from the dust sources of southeastern Iraq. In this way, the establishment of a trough (Naveh) on these areas will cause divergence on the surface of the earth and pick up particles that enter Iran through Arabian winds (Figure 8b). Comparing the findings of this study with those of [50–52, 66] and [25], it is planned. The tracking of dust at two altitudes of 500 and 1,000 m above the surface in the period of 24 hr before the target time has been examined in this study using data from the Global Data Assimilation System (Figure 7).

5. Conclusions

The presence of dust, particularly in the western parts of Iran, has become one of Iran's environmental challenges in recent years. Every year, the phenomenon of dust commonly affects the western part of Iran. The current study employed the reflective and thermal characteristics of MODIS data in both the cold and hot seasons to examine the dust masses entering Iran from the southwest. Additionally, this study simultaneously examined the use of reflecting and thermal properties for dust detection using MODIS satellite imagery. The findings were applied to enhance the synoptic analysis of dust occurrence, and the HYSPLIT model was employed to describe the dust origin.

Reflective characteristics were utilized for identifying dust for a very long time, and this has given rise to indices like NDDI. However, because this index does not employ near-infrared wavelengths, it is unable to differentiate between dusts over water bodies and performs poorly when separating dust from the desert and other arid regions. As a result, dust identification is made simpler when employing the near-infrared range, particularly when the image incorporates deserts and other arid regions. Numerous times, the thermal features in the 3.959, 8.55, 11.03, and 12.02 m spectral ranges—each of which can be applied in various environments—were taken into consideration. The study's findings demonstrated that employing these features separately in situations with complicated terrain (such as when there is dust in the air, water, and land, as well as desert, bare land, and vegetation in the image) does not yield good results. In the meanwhile, their use can effectively isolate the dust pixels from other occurrences by applying specific thresholds. Therefore, the best way to detect dust in complicated surroundings is to simultaneously exploit reflective and thermal properties. In synoptic meteorological conditions, lower G850 (1,430 gpm) and MSLP (1005) values across the Levantine basin, Syria–Iraq to the southwest, and Central Asia dynamically increase ascending conditions along the troposphere. Strong Shamal winds from the northwest and pro-generated northerlies from the eastern Mediterranean combined to produce a bigger dust-AOD hotspot over southwest Iran. On a chilly day, however, the persistent high pressure, a subtropical jet (>56 ms^{-1}), and geopotential values at 500 hPa exacerbate the air subsidence, modulating anticyclonic wind pattern, causing considerable dust accumulation in Arabia and southwest Iran. The combined examination of dust characteristics provides the possibility of its comprehensive study. The present research showed that the use of satellite imagery in combination with synoptic findings and atmospheric transport and dispersion models can be used in the best way to provide the mechanism of formation and transfer of dust.

Data Availability

The data used to support the findings of this study are available from the corresponding author upon request.

Conflicts of Interest

The authors declare that they have no conflicts of interest.

Acknowledgments

This research was financially supported by the Iran National Science Foundation (INSF) through research project no. 95827182.

References

[1] N. Middleton, "Variability and trends in dust storm frequency on decadal timescales: climatic drivers and human impacts," *Geosciences*, vol. 9, no. 6, Article ID 261, 2019.

[2] T. M. Nodej and M. Rezazadeh, "The spatial distribution of critical wind erosion centers according to the dust event in Hormozgan province (south of Iran)," *Catena*, vol. 167, pp. 340–352, 2018.

[3] A. Rashki, M. Arjmand, and D. G. Kaskaoutis, "Assessment of dust activity and dust-plume pathways over Jazmurian Basin, Southeast Iran," *Aeolian Research*, vol. 24, pp. 145–160, 2017.

[4] M. Rezaei, M. Farajzadeh, T. Mielonen, and Y. Ghavidel, "Analysis of spatio-temporal dust aerosol frequency over Iran based on satellite data," *Atmospheric Pollution Research*, vol. 10, no. 2, pp. 508–519, 2019.

[5] M. V. Sivakumar, "Impacts of sand storms/dust storms on agriculture," in *Natural Disasters and Extreme Events in Agriculture*, pp. 159–177, Springer, Berlin, Heidelberg, 2005.

[6] T. Takemi and N. Seino, "Dust storms and cyclone tracks over the arid regions in east Asia in spring," *Journal of Geophysical Research*, vol. 110, no. D18, 2005.

[7] J. M. Prospero, P. Ginoux, O. Torres, S. E. Nicholson, and T. E. Gill, "Environmental characterization of global sources of atmospheric soil dust identified with the Nimbus 7 total ozone mapping spectrometer (TOMS) absorbing aerosol product," *Reviews of Geophysics*, vol. 40, no. 1, pp. 2-1–2-31, 2002.

[8] H. Shen, J. Abuduwaili, A. Samat, and L. Ma, "A review on the research of modern Aeolian dust in Central Asia," *Arabian Journal of Geosciences*, vol. 9, pp. 1–16, 2016.

[9] R. Mao, Z. Hu, C. Zhao, D.-Y. Gong, D. Guo, and G. Wu, "The source contributions to the dust over the tibetan plateau: a modelling analysis," *Atmospheric Environment*, vol. 214, Article ID 116859, 2019.

[10] L. Shi, J. Zhang, F. Yao, D. Zhang, and H. Guo, "Drivers to dust emissions over dust belt from 1980 to 2018 and their variation in two global warming phases," *Science of The Total Environment*, vol. 767, Article ID 144860, 2021.

[11] T. X. P. Zhao, S. Ackerman, and W. Guo, "Dust and smoke detection for multi-channel imagers," *Remote Sensing*, vol. 2, no. 10, pp. 2347–2368, 2010.

[12] W. E. Shenk and R. J. Curran, "The detection of dust storms over land and water with satellite visible and infrared measurements," *Monthly Weather Review*, vol. 102, no. 12, pp. 830–837, 1974.

[13] S. A. Ackerman, "Global satellite observations of negative brightness temperature differences between 11 and 6.7 μm," *Journal of the Atmospheric Sciences*, vol. 53, no. 19, pp. 2803–2812, 1996.

[14] S. D. Miller, "A consolidated technique for enhancing desert dust storms with MODIS," *Geophysical Research Letters*, vol. 30, no. 20, 2003.

[15] B. Chen, P. Zhang, B. Zhang et al., "An overview of passive and active dust detection methods using satellite measurements," *Journal of Meteorological Research*, vol. 28, no. 6, pp. 1029–1040, 2014.

[16] J. Huang, J. Ge, and F. Weng, "Detection of Asia dust storms using multisensor satellite measurements," *Remote Sensing of Environment*, vol. 110, no. 2, pp. 186–191, 2007.

[17] L. Klüser and K. Schepanski, "Remote sensing of mineral dust over land with MSG infrared channels: a new bitemporal mineral dust index," *Remote Sensing of Environment*, vol. 113, no. 9, pp. 1853–1867, 2009.

[18] P. Baghbanan, Y. Ghavidel, and M. Farajzadeh, "Spatial analysis of spring dust storms hazard in Iran," *Theoretical and Applied Climatology*, vol. 139, no. 3-4, pp. 1447–1457, 2020.

[19] J. Barkan and P. Alpert, "Synoptic analysis of a rare event of Saharan dust reaching the Arctic region," *Weather*, vol. 65, no. 8, pp. 208–211, 2010.

[20] Y. Chun, K. O. Boo, J. Kim, S. U. Park, and M. Lee, "Synopsis, transport, and physical characteristics of Asian dust in Korea," *Journal of Geophysical Research*, vol. 106, no. D16, pp. 18461–18469, 2001.

[21] A. Ghasem, A. Shamsipour, M. Miri, and T. Safarrad, "Synoptic and remote sensing analysis of dust events in southwestern Iran," *Natural Hazards*, vol. 64, no. 2, pp. 1625–1638, 2012.

[22] M. Hamidi, M. R. Kavianpour, and Y. Shao, "Synoptic analysis of dust storms in the Middle East," *Asia-Pacific Journal of atmospheric sciences*, vol. 49, pp. 279–286, 2013.

[23] N. Brooks and M. Legrand, "Dust variability over Northern Africa and rainfall in the Sahel," in *Linking Land Surface Change to Climate Change*, Springer, Dordrecht, 2000.

[24] J. J. Qu, X. Hao, M. Kafatos, and L. Wang, "Asian dust storm monitoring combining terra and aqua MODIS SRB measurements," *IEEE Geoscience and Remote Sensing Letters*, vol. 3, no. 4, pp. 484–486, 2006.

[25] Q. Azizi, M. Miri, and S. O. Nabavi, "Dust detection in the western half of Iran," *Geographical Studies of Arid Areas*, vol. 2, no. 7, pp. 63–81, 2012.

[26] K. Raispour, M. Khosravi, T. Tavousi, and M. Sharifikiya, "The influence of the polar front jet stream on the formation of dust events in the southwest of Iran," *Air Quality, Atmosphere & Health*, vol. 9, no. 1, pp. 15–23, 2016.

[27] P. Ginoux, J. M. Prospero, T. E. Gill, N. C. Hsu, and M. Zhao, "Global-scale attribution of anthropogenic and natural dust sources and their emission rates based on MODIS Deep Blue aerosol products," *Reviews of Geophysics*, vol. 50, no. 3, 2012.

[28] M. Rezazadeh, P. Irannejad, and Y. Shao, "Climatology of the Middle East dust events," *Aeolian Research*, vol. 10, pp. 103–109, 2013.

[29] E. E. Houssos, T. Chronis, A. Fotiadi, and F. Hossain, "Atmospheric circulation characteristics favoring dust outbreaks over the solar village, central Saudi Arabia," *American Meteorological Society*, vol. 143, pp. 3263–3275, 2015.

[30] S. O. Nabavi, L. Haimberger, and C. Samimi, "Sensitivity of WRF-chem predictions to dust source function specification in West Asia," *Aeolian Research*, vol. 24, pp. 115–131, 2017.

[31] L. Hermida, A. Merino, J. L. Sánchez, S. Fernández-González, E. García-Ortega, and L. López, "Characterization of synoptic patterns causing dust outbreaks that affect the Arabian Peninsula," *Atmospheric Research*, vol. 199, pp. 29–39, 2018.

[32] A. Rashki, D. G. Kaskaoutis, A. Mofidi et al., "Effects of monsoon, Shamal and Levar winds on dust accumulation over the Arabian Sea during summer—the July 2016 case," *Aeolian Research*, vol. 36, pp. 27–44, 2019.

[33] A. M. Awad and A.-W. S. Mashat, "Synoptic features associated with dust transition processes from North Africa to Asia," *Arabian Journal of Geosciences*, vol. 7, pp. 2451–2467, 2013.

[34] A. M. Awad and A.-W. S. Mashat, "Synoptic characteristics of spring dust days over northern Saudi Arabia," *Air Quality Atmosphere & Health*, vol. 9, no. 1, pp. 41–50, 2016.
[35] A. A. Attiya and B. G. Jones, "Climatology of Iraqi dust events during 1980–2015," *SN Applied Sciences*, vol. 2, Article ID 845, 2020.
[36] D. Gholamzade Ledari, M. Hamidi, and Y. Shao, "Evaluation of the 13 April 2011 frontal dust storm in West Asia," *Aeolian Research*, vol. 44, Article ID 100592, 2020.
[37] K. Mohammadpour, M. Sciortino, D. G. Kaskaoutis, and A. Rashki, "Classification of synoptic weather clusters associated with dust accumulation over southeastern areas of the caspian sea (Northeast Iran and Karakum desert)," *Aeolian Research*, vol. 54, Article ID 100771, 2022.
[38] N. H. Hamzeh, S. Karami, D. G. Kaskaoutis, I. Tegen, M. Moradi, and C. Opp, "Atmospheric dynamics and numerical simulations of six frontal dust storms in the Middle East region," *Atmosphere*, vol. 12, no. 1, Article ID 125, 2021.
[39] M. Hamidianpour, S. M. A. Jahanshahi, D. G. Kaskaoutis, A. Rashki, and P. G. Nastos, "Climatology of the Sistan Levar wind: atmospheric dynamics driving its onset, duration and withdrawal," *Atmospheric Research*, vol. 260, Article ID 105711, 2021.
[40] S. Karami, D. G. Kaskaoutis, S. S. Kashani, M. Rahnama, and A. Rashki, "Evaluation of nine operational models in forecasting different types of synoptic dust events in the Middle East," *Geosciences*, vol. 11, no. 11, Article ID 458, 2021.
[41] H. Hersbach, B. Bell, P. Berrisford et al., "The ERA5 global reanalysis," *Quarterly Journal of the Royal Meteorological Society*, vol. 146, no. 730, pp. 1999–2049, 2020.
[42] A. Inness, F. Baier, A. Benedetti et al., "The MACC reanalysis: an 8 year data set of atmospheric composition," *Atmospheric Chemistry and Physics*, vol. 13, no. 8, pp. 4073–4109, 2013.
[43] J.-J. Morcrette, O. Boucher, L. Jones et al., "Aerosol analysis and forecast in the European centre for medium-range weather forecasts integrated forecast system: forward modeling," *Journal of Geophysical Research*, vol. 114, no. D6, Article ID D06206, 2009.
[44] A. Benedetti, J. J. Morcrette, O. Boucher et al., "Aerosol analysis and forecast in the European centre for medium-range weather forecasts integrated forecast system: forward modeling," *Journal of Geophysical Research: Atmospheres*, vol. 114, no. D6, 2009.
[45] Q. Jin, J. Wei, W. K. M. Lau, B. Pu, and C. Wang, "Interactions of Asian mineral dust with Indian summer monsoon: recent advances and challenges," *Earth-Science Reviews*, vol. 215, Article ID 103562, 2021.
[46] https://search.earthdata.nasa.gov.
[47] Y. Liu, R. Liu, and X. Cheng, "Dust detection over desert surfaces with thermal infrared bands using dynamic reference brightness temperature differences," *Journal of Geophysical Research: Atmospheres*, vol. 118, no. 15, pp. 8566–8584, 2013.
[48] M. Hennen, K. White, and M. Shahgedanova, "An assessment of SEVIRI imagery at different temporal resolutions and the effect on accurate dust emission mapping," *EGU General Assembly Conference Abstracts*, vol. 19, Article ID 9974, 2017.
[49] "Dust storm over the Persian Gulf," 2008, https://earthobservatory.nasa.gov/images/20175/dust-storm-over-the-Persian-gulf.
[50] D. G. Kaskaoutis, E. E. Houssos, A. Rashki et al., "The Caspian Sea-Hindu Kush Index (CasHKI): a regulatory factor for dust activity over southwest Asia," *Global and Planetary Change*, vol. 137, pp. 10–23, 2016.
[51] K. Mohammadpour, M. Sciortino, and D. G. Kaskaoutis, "Classification of weather clusters over the Middle East associated with high atmospheric dust-AODs in West Iran," *Atmospheric Research*, vol. 259, Article ID 105682, 2021a.
[52] K. Mohammadpour, M. Sciortino, M. Saligheh, T. Raziei, and A. Darvishi Boloorani, "Spatiotemporal regionalization of atmospheric dust based on multivariate analysis of MACC model over Iran," *Atmospheric Research*, vol. 249, Article ID 105322, 2021b.
[53] J. Sciare, K. Oikonomou, O. Favez et al., "Long-term measurements of carbonaceous aerosols in the Eastern Mediterranean: evidence of long-range transport of biomass burning," *Atmospheric Chemistry and Physics*, vol. 8, no. 18, pp. 5551–5563, 2008.
[54] D. Francis, J. P. Chaboureau, N. Nelli et al., "Summertime dust storms over the Arabian Peninsula and impacts on radiation, circulation, cloud development and rain," *Atmospheric Research*, vol. 250, Article ID 105364, 2021.
[55] D. G. Kaskaoutis, A. Rashki, E. E. Houssos et al., "Meteorological aspects associated with dust storms in the Sistan region, Southeastern Iran," *Climate Dynamics*, vol. 45, pp. 407–424, 2015a.
[56] D. G. Kaskaoutis, A. Rashki, P. Francois, U. C. Dumka, E. E. Houssos, and M. Legrand, "Meteorological regimes modulating dust outbreaks in Southwest Asia: the role of pressure anomaly and inter-tropical convergence zone on the 1–3 July 2014 case," *Aeolian Research*, vol. 18, pp. 83–97, 2015b.
[57] P. Banerjee, S. K. Satheesh, and K. K. Moorthy, "The unusual severe dust storm of May 2018 over Northern India: genesis, propagation and associated conditions," *Journal of Geophysical Research Atmospheres*, vol. 126, no. 7, Article ID e2020JD032369, 2021.
[58] S. Namdari, N. Karimi, A. Sorooshian, G. H. Mohammadi, and S. Sehatkashani, "Impacts of climate and synoptic fluctuations on dust storm activity over the Middle East," *Atmospheric Environment*, vol. 173, pp. 265–276, 2018.
[59] "Dust storm over the Persian Gulf," 2017, https://earthobservatory.nasa.gov/images/89705/dust-over-the-persian-gulf.
[60] P. G. Thoppil and P. J. Hogan, "Persian Gulf response to a wintertime shamal wind event," *Deep Sea Research Part I: Oceanographic Research Papers*, vol. 57, no. 8, pp. 946–955, 2010.
[61] F. Abdi Vishkaee, C. Flamant, J. Cuesta, L. Oolman, P. Flamant, and H. R. Khalesifard, "Dust transport over Iraq and northwest Iran associated with winter Shamal: a case study," *Journal of Geophysical Research: Atmospheres*, p. 117 (D3), 2021.
[62] D. G. Ledari, M. Hamidi, and Y. Shao, "Numerical simulation of the 18 February 2017 frontal dust storm over southwest of Iran using WRF-Chem, satellite imagery, and PM10 concentrations," *Journal of Arid Environments*, vol. 196, Article ID 104637, 2022.
[63] H. Salmabadi, R. Khalidy, and M. Saeedi, "Transport routes and potential source regions of the Middle Eastern dust over Ahvaz during 2005–2017," *Atmospheric Research*, vol. 241, Article ID 104947, 2020.
[64] A. F. Stein, R. R. Draxler, G. D. Rolph, B. J. B. Stunder, M. D. Cohen, and F. Ngan, "NOAA's HYSPLIT atmospheric transport and dispersion modeling system," *Bulletin of the American Meteorological Society*, vol. 96, pp. 2059–2077, 2015.
[65] https://www.arl.noaa.gov.
[66] R. Modarres and S. Sadeghi, "Spatial and temporal trends of dust storms across desert regions of Iran," *Natural Hazards*, vol. 90, no. 1, pp. 101–114, 2018.

[67] E. Ganor, A. Stupp, I. Osetinsky, and P. Alpert, "Synoptic classification of lower troposphere profiles for dust days," *Journal of Geophysical Research*, vol. 115, no. D11, 2010.
[68] N. J. Middleton, "Desert dust hazards: a global review," *Aeolian Research*, vol. 24, pp. 53–63, 2017.
[69] A. Rashki, D. G. Kaskaoutis, and A. Sepehr, "Statistical evaluation of the dust events at selected stations in southwest Asia: from the Caspian Sea to the Arabian sea," *Catena*, vol. 165, pp. 590–603, 2018.
[70] Y. Shao and C. H. Dong, "A review on East Asian dust storm climate modelling and monitoring," *Global and Planetary Change*, vol. 52, no. 1-4, pp. 1–22, 2006.